Steel and Composite Structures, *Vol. 16, No. 6 (2014) 559-576*
DOI: http://dx.doi.org/10.12989/scs.2014.16.6.559

Non-linear analysis of side-plated RC beams considering longitudinal and transversal interlayer slips

Jerneja Kolšek [2], Tomaž Hozjan [1], Aleš Kroflič [1], Miran Saje [*1] and Igor Planinc [1]

[1] *University of Ljubljana, Faculty of Civil and Geodetic Engineering, Jamova 2, SI-1115 Ljubljana, Slovenia*
[2] *ZAG - Slovenian National Building and Civil Engineering Institute, Dimičeva 12, SI-1000 Ljubljana, Slovenia*

(*Received July 29, 2011, Revised October 21, 2013, Accepted January 15, 2014*)

Abstract. A new mathematical model and its finite element formulation for the non-linear stress-strain analysis of a planar beam strengthened with plates bolted or adhesively bonded to its lateral sides is presented. The connection between the layers is considered to be flexible in both the longitudinal and the transversal direction. The following assumptions are also adopted in the model: for each layer (i.e., the beam and the side plates) the geometrically linear and materially non-linear Bernoulli's beam theory is assumed, all of the layers are made of different homogeneous non-linear materials, the debonding of the beam from the side-plates due to, for example, a local buckling of the side plate, is prevented. The suitability of the theory is verified by the comparison of the present numerical results with experimental and numerical results from literature. The mechanical response arising from the theoretical model and its numerical formulation has been found realistic and the numerical model has been proven to be reliable and computationally effective. Finally, the present formulation is employed in the analysis of the effects of two different realizations of strengthening of a characteristic simply supported flexural beam (plates on the sides of the beam versus the tension-face plates). The analysis reveals that side plates efficiently enhance the bearing capacity of the flexural beam and can, in some cases, outperform the tensile-face plates in a lower loss of ductility, especially, if the connection between the beam and the side plates is sufficiently stiff.

Keywords: externally plated beam; side-plated beam; tension-face plated beam; longitudinal and transverse slips; Reissner beam; reinforced concrete beam; numerical model

1. Introduction

Over the course of the past few decades the plating technique as one of the peak engineering solutions of strengthening of flexural beams gained popularity in design of structural retrofitting and building renovation. Although a range of different plating solutions is currently available for the implementation in the engineering practice, the tension-face plating technique is applied as a rule. While often mistakenly considered as less efficient, alternative side-plating techniques are considered to be a second choice where the tension face plates are not applicable due to structural or aesthetic reasons.

Reinforced concrete (RC) beams may fail in flexure or shear. The shear failure is brittle whereas the flexural failure is mostly ductile. In order to achieve the ductile response, the RC

*Corresponding author, Professor, E-mail: msaje@fgg.uni-lj.si

http://www.techno-press.org/?journal=scs&subpage=8 ISSN: 1229-9367 (Print), 1598-6233 (Online)

beams are designed in the way that their flexural ductility is large at extreme loading. The request for high ductility initiated an intensive research in the late nineties (e.g., Ahmed 1996, Oehlers *et al*. 2000, Nguyen *et al*. 2001, Oehlers and Seracino 2004, Liu *et al*. 2006) that revealed that tension-face plates may in some cases severely restrict the ductility of the retrofitted elements, while the side plates, by the contrast, can prove to be a better choice in this respect. Furthermore, it became clear that, for a sufficient understanding of the phenomenon of ductility, we need to research further into this matter by performing extensive experimental as well as computational parametric studies.

The theory of externally strengthened (plated) flexural beams originates from the theory of multi-layer beams dating back to the middle of the previous century. An extensive overview of the work in this field was presented, e.g., in Čas *et al*. 2004a, b, Kroflič *et al*. 2010a, b, Milner and Tan 2001, Ranzi *et al*. 2006, Schnabl *et al*. 2006, 2007. However, due to their unique form of failure, the standard composite beam theory is directly applicable only to a small range of plated beam problems. For the tension-face strengthened RC flexural beams, for example, failure may occur due to an excessive longitudinal contact stress or due to the transverse debonding of the beam from the plate. For the mathematical description of such a failure, the present computational models for the analysis of standard composite beams considering not only the interlayer slip but also the interlayer uplift may be directly applicable. Because the effect of the uplift is negligible in the vast majority of multi-layer beams, such models, however, are rare and have been introduced only recently (e.g., Alfano and Crisfield 2001, Thomsen *et al*. 2004, Gara *et al*. 2006, Ranzi *et al*. 2006, Pan and Leung 2008). For less conventional types of the external strengthening techniques like the side plating technique, a pronounced transversal partial interaction occurs as well, which demands a somewhat different consideration. Oehlers *et al*. (1997) seem to be the first to discuss mathematically the combined effect of both longitudinal and transversal slips between the components of the side-plated beams. Their model was derived with the aim to provide adequate design rules including the adaptation of the standard rigid plastic analysis and the methods for preventing premature buckling of plates (Smith *et al*. 1999a, b) or an early failure of bolt-shear connectors (Ahmed 1996). The non-linear numerical method for the bolted side-plated beams was first presented by Siu and Su (2011). Their method considers the material non-linearity and inelastic behaviour of the bolted connection, as well as both the longitudinal and the transversal partial interaction.

Here a new finite element formulation for the materially non-linear stress-strain analysis of beams strengthened with two longitudinal side plates is presented. The method is based upon a planar beam model of Reissner (1972) assuming linearized kinematics. The basic variables in this finite-element formulation are strains. The Galerkin-type of the finite element formulation is employed as in Planinc *et al*. (2001). The present article is a substantive continuation of the research work presented in Kolšek *et al*. (2013), where an analytical solution of side-plated elastic beams is presented. The present model considers the following assumptions: (i) shear deformations are neglected in the kinematic equations, but shear stresses are considered via equilibrium equations; (ii) the beam and the side plates have constant cross-sections and straight axes; (iii) the layers are made of different yet homogeneous non-linear materials; (iv) the bond between the layers is flexible enough to allow for small slips (the longitudinal and the transversal) to occur at the side plate/beam contact; (v) uplifting and impressing of one layer against the other are neglected; (vi) the interaction between the layers is typically realized through a bonding layer of an infinitesimal thickness, which can be, hence, neglected in the model; and (vii) the contact connection is supposed to behave non-linearly. The iterative solution procedure employs the

Newton-Raphson method and is load-controlled.

The numerical solution of the present model is compared to the experimental results of Su *et al*. (2010) and Siu and Su (2010) as well as to the numerical results of Siu and Su (2011). Finally, effects of the different strengthening arrangements on an RC flexural beam are presented and discussed. Conclusions are given in the last section.

2. Mathematical model

2.1 Preliminaries

We consider a planar straight beam '*a*' of length L^a with two symmetrically bonded side plates '*b*' of length L^b. The cross-sections of the beam and the side-plates, A_x^a and A_x^b, are constant throughout their lengths. Deformations of the plated beam are described in the (*X*,*Z*)-plane of a fixed spatial right-handed Cartesian coordinate system (*X*, *Y*, *Z*) with the orthonormal base vectors E_X, E_Z and $E_Y = E_Z \times E_X$. The local coordinate systems of the beam and the side plates are identical and, in the initial undeformed state, coincide with the spatial coordinate system. The local coordinates are marked by $x^a \equiv x^b \equiv x$, $y^a \equiv y^b \equiv y$, and $z^a \equiv z^b \equiv z$, where the upper indices $(\bullet)^a$ and $(\bullet)^b$ refer to the beam and the side plates, respectively. The undeformed and the deformed configurations, the typical cross-sections and the loading of the plated beam are depicted in Fig. 1.

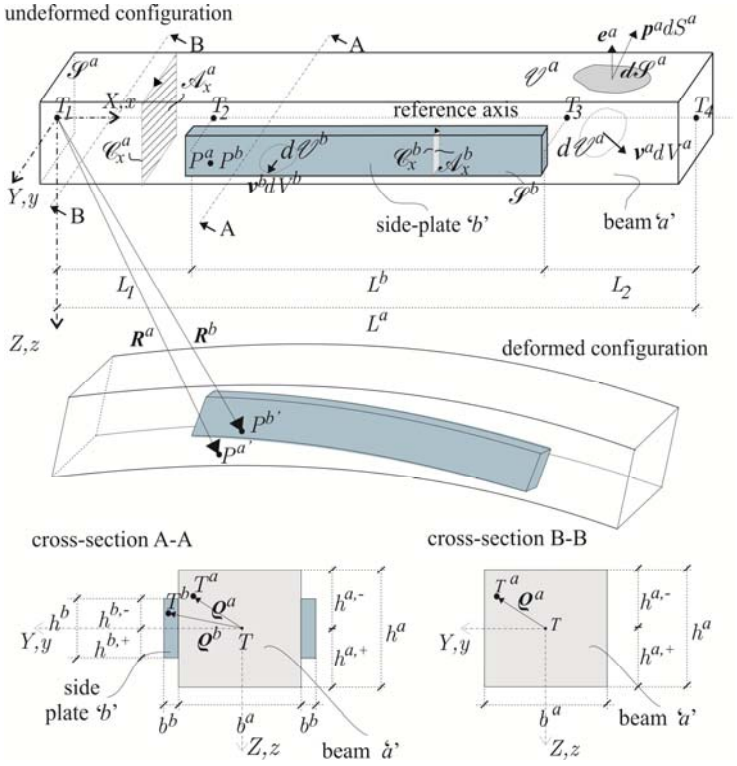

Fig. 1 Undeformed and deformed configurations of a side-plated beam

The beam and the side-plates are bonded one to another with discrete connectors (e.g., bolts) or with an adhesive bonding layer of a small thickness. In either of the two cases, the connection is not perfectly rigid, yielding the longitudinal and the transversal slips between the side plate and the beam to evolve along the contact area once the beam has been deformed.

Both the side plates and the beam are modelled by the linearized planar beam theory of Reissner (1972). The shear strains are neglected in the kinematic equations, which is a reasonable assumption for slender beams (Schnabl *et al*. 2007).

The mathematical model of the side-plated beam in Fig. 1 hence consists of three unplated beams spanning the parts $\overline{T_1T_2}$, $\overline{T_2T_3}$ and $\overline{T_3T_4}$ of the reference axis, and two plated beams located eccentrically on the part $\overline{T_2T_3}$ of the reference axis. Due to the symmetry of the plate arrangement and in view of the assumption of the planar deformation, the two plates can be considered as one eccentric plate with a double thickness. The final mathematical model of the side-plated beam as studied in the present paper is thus described by an unplated beam of length L^a to which a plate of the double thickness is bonded eccentrically, using an inelastic adhesive.

2.2 Governing equations

Only the governing equations of the plated part of the model are presented. The equations of the non-plated parts easily follow by neglecting the corresponding terms of the plates.

The governing equations of the plated part consist of kinematic, equilibrium and constitutive equations, each written separately for the beam ($i = a$) and the side plates ($i = b$) (Hjelmstad 2005)

$$\begin{aligned} u^{i\prime} - \varepsilon^i &= 0, \\ w^{i\prime} + \varphi^i &= 0, \\ \phi^{i\prime} - \kappa^i &= 0, \end{aligned} \tag{1}$$

$$\begin{aligned} N^{i\prime} + P_x{}^i &= 0, \\ Q^{i\prime} + P_z{}^i &= 0, \\ M^{i\prime} - Q^i + M_y{}^i &= 0, \end{aligned} \tag{2}$$

$$\begin{aligned} N^i &= \int_{A_x{}^i} \sigma^i dA_x^i, \\ M^i &= \int_{A_x{}^i} z\sigma^i dA_x^i. \end{aligned} \tag{3}$$

In Eqs. (1)-(3) $(\bullet)'$ denotes the derivative with respect to material coordinate x, while u^i, w^i and φ^i are, respectively, the X-displacement, the Z-displacement and the rotation of the reference axis of layer 'i' ($i = a, b$). ε^i and κ^i denote the extensional and the bending strain (the curvature) of the reference axis and N^i, Q^i and M^i refer to stress resultants (the axial force, the shear force and the bending moment). $P_x{}^i$, $P_z{}^i$ and $M_y{}^i$ are the components of the traction vector per unit of the reference axis of layer 'i', and statically reduced with respect to the reference axis. In fact, they are static equivalents of surface and volume forces, $\boldsymbol{p}^i$ and $\boldsymbol{v}^i$, after being reduced to the beam reference axis ($i = a, b$), see, e.g., Hjelmstad (2005)

$$P^i = \int_{C_x^i} \boldsymbol{p}^i dc_x + \int_{A_x^i} \boldsymbol{v}^i dA_x,$$
$$M^i = \int_{C_x^i} \boldsymbol{\rho}^i \times \boldsymbol{p}^i dc_x + \int_{A_x^i} \boldsymbol{\rho}^i \times \boldsymbol{v}^i dA_x. \tag{4}$$

The graphical description of the quantities in Eq. (4) is also given in Fig. 1. Furthermore, due to the beam-plate contact, the contributions of not only the external tractions, but also of the contact tractions have to be considered in Eq. (4). The *X*-, *Y*- and *Z*-components of the traction vectors $\boldsymbol{P}^i$ and $\boldsymbol{M}^i$ are, therefore, the sum of their external and contact counterparts

$$\begin{aligned} P_x^{\ i} &= P_{e,x}^{\ i} + P_{c,x}^{\ i}, \\ P_z^{\ i} &= P_{e,z}^{\ i} + P_{c,z}^{\ i}, \\ M_y^{\ i} &= M_{e,y}^{\ i} + M_{c,y}^{\ i}, \end{aligned} \tag{5}$$

where indices '*e*' and '*c*' refer to the external and contact traction contributions.

In the sequel a more detailed consideration of the contact parts of the traction vectors (i.e., $P_{c,x}^{\ i}$, $P_{c,z}^{\ i}$ and $M_{c,y}^{\ i}$) is presented. Because we assume that each layer of the beam only deforms in the (*X*, *Z*)-plane, the *Y*-component of the contact traction equals zero. Next, the intensity of the contact traction depends on the contact connection stiffness dictating the size of the slip between the layers. The slip is represented by the relative displacement between the beam and the side plates. If we imagine two initially coincident particles, P^a and P^b (see Fig. 1), we may easily perceive that their positions with regard to the fixed coordinate system are different after the structure has been deformed. Their new, deformed position vectors are ($i = a, b$)

$$\boldsymbol{R}^i = X^i \boldsymbol{E}_X + Y^i \boldsymbol{E}_Y + Z^i \boldsymbol{E}_Z. \tag{6}$$

The spatial coordinates X^i, Y^i and Z^i depend on the displacement vector of each particle and the particular layer rotation, u^i , w^i and φ^i ($i = a, b$), and are given by

$$\begin{aligned} X^a &= x + u^a + z\varphi^a, \quad & X^b &= x + u^b + z\varphi^b \\ Z^a &= w^a, & Z^b &= w^b. \end{aligned} \tag{7}$$

The slip vector between the two particles of the beam and the side plate being initially in contact and having coordinates (x, y, z) is thus

$$\begin{aligned} [[\boldsymbol{R}]] &= \boldsymbol{R}^b - \boldsymbol{R}^a = \Delta U \boldsymbol{E}_X + \Delta W \boldsymbol{E}_Z, \\ \Delta U &= u^b - u^a + z\left(\varphi^b - \varphi^a\right), \\ \Delta W &= w^b - w^a. \end{aligned} \tag{8}$$

The magnitudes of the contact tractions are highly dictated by the type of the actual interface connection. Here we assume that there is no correlation between the slips in the $X-$ and $Z-$ directions. A general non-linear relationship between the slip and the related contact traction in each direction is assumed as

$$\boldsymbol{p}_c^i = \begin{Bmatrix} p_{c,x}^i \\ p_{c,z}^i \end{Bmatrix} = \begin{Bmatrix} f(\Delta U) \\ g(\Delta W) \end{Bmatrix}. \tag{9}$$

Functions f and g depend on the type of contact materials and the technical details of the connection. They must be determined by experiments for the actual type of the connection. After inserting the contact traction load, Eq. (9), into Eq. (4) and considering that the contact tractions $\boldsymbol{P}^a$ and $\boldsymbol{P}^b$ (and likewise $\boldsymbol{M}^a$ and $\boldsymbol{M}^b$) have the opposite sign, we end up with

$$\begin{Bmatrix} \boldsymbol{P}_{c,x}^a \\ \boldsymbol{P}_{c,z}^a \\ \boldsymbol{M}_{c,y}^a \end{Bmatrix} = \begin{Bmatrix} -\boldsymbol{P}_{c,x}^b \\ -\boldsymbol{P}_{c,z}^b \\ -\boldsymbol{M}_{c,y}^b \end{Bmatrix} = \begin{Bmatrix} 2\int_{-h^{b,-}}^{h^{b,+}} p_{c,x}\, dz \\ 2\int_{-h^{b,-}}^{h^{b,+}} p_{c,z}\, dz \\ 2\int_{-h^{b,-}}^{h^{b,+}} z\, p_{c,x}\, dz \end{Bmatrix} = \begin{Bmatrix} \boldsymbol{F}\ (\Delta U) \\ \boldsymbol{G}\ (\Delta W) \\ \boldsymbol{H}\ (\Delta U) \end{Bmatrix}. \tag{10}$$

When $\boldsymbol{P}_{c,x}^i$, $\boldsymbol{P}_{c,z}^i$ and $\boldsymbol{M}_{c,y}^i$ from Eq. (10) are substituted in Eq. (5), the system of equations of the side-plated beam, Eqs. (1)-(3), consists of 4 non-linear algebraic and 12 quasi-linear ordinary first-order differential equations. The analytical solution of the problem is only possible when both the material models and the contact laws are linear (Kolšek *et al*. 2013). Otherwise a numerical method has to be employed. The finite element method is employed here as shortly described in the next section.

3. The finite element formulation

The strain-based finite element method is employed as described in detail in Čas *et al*. (2004a, b) and Kroflič *et al*. (2010b). This innovative variant of the finite-element method is based on the modified principle of virtual work with the strains as the only interpolated unknown functions of the problem, while the remaining primary unknowns appear solely as boundary values in the functional

$$\begin{aligned} \delta W^* = \sum_{i=a}^{b} \delta W^{i*} = \\ \int_0^{L^i} \left(\left(N_c^i - N^i \right) \delta \varepsilon^i + \left(M_c^i - M^i \right) \delta \kappa^i \right) dx^i + \\ + \left(u^i\left(L^i\right) - u^i(0) - \int_0^{L^i} \varepsilon^i d\xi \right) \delta N^i(0) + \left(w^i\left(L^i\right) - w^i(0) + \int_0^{L^i} \varphi^i d\xi \right) \delta Q^i(0) + \\ \left(\varphi^i\left(L^i\right) - \varphi^i(0) - \int_0^{L^i} \kappa^i d\xi \right) \delta M^i(0) + \left(-S_1^i - N^i(0) \right) \delta u^i(0) + \end{aligned} \tag{11}$$

$$\begin{aligned}\left(-S_2^i - Q^i(0)\right)\delta w^i(0) + \left(-S_3^i - M^i(0)\right)\delta\varphi^i(0) + \left(S_4^i - N^i(L)\right)\delta u^i(L) + \\ \left(S_5^i - Q^i(L)\right)\delta w^i(L) + \left(S_6^i - M^i(L)\right)\delta\varphi^i(L).\end{aligned} \tag{11}$$

As observed from the functional, the strains $\varepsilon^i(x)$ and $\kappa^i(x)$, the generalized boundary forces $N^i(0)$, $Q^i(0)$ and $M^i(0)$ and the boundary kinematic quantities $u^i(0)$, $u^i(L)$, $w^i(0)$, $w^i(L)$, $\varphi^i(0)$ and $\varphi^i(L)$ ($i = a, b$) represent the set of the primary unknowns of the problem. Here only $\varepsilon^i(x)$ and $\kappa^i(x)$ are functions of x. They are interpolated with the Lagrangian polynomials L_m ($m = 1, 2, ..., M$) of the order ($M-1$) as

$$\varepsilon^i(x) = \sum_{m=1}^{M} L_m(x)\varepsilon_m^i, \quad \kappa^i(x) = \sum_{m=1}^{M} L_m(x)\kappa_m^i, \tag{12}$$

where ε_m^i and κ_m^i are the unknown scalar nodal values of the extensional and bending strains of layers $i = a, b$. The interpolation points are taken to be equidistant. After inserting $\varepsilon^i(x)$ and $\kappa^i(x)$ from Eq. (12) into Eq. (11), we obtain the following system of discrete equilibrium equations of the side-plated beam accounting for longitudinal and transverse contact slips ($m = 1, 2, ..., M$)

$$\begin{aligned}
g_m &= \int_0^{L^a} \left(N_c^a - N^a\right) L_m \, dx = 0, & g_{M+m} &= \int_0^{L^b} \left(N_c^b - N^b\right) L_m \, dx = 0, \\
g_{2M+m} &= \int_0^{L^a} \left(M_c^a - M^a\right) L_m \, dx = 0, & g_{3M+m} &= \int_0^{L^b} \left(M_c^b - M^b\right) L_m \, dx = 0, \\
g_{4M+1} &= u^a\left(L^a\right) - u^a(0) - \int_0^{L^a} \varepsilon^a dx = 0, & g_{4M+2} &= u^b\left(L^b\right) - u^b(0) - \int_0^{L^b} \varepsilon^b dx = 0, \\
g_{4M+3} &= w^a\left(L^a\right) - w^a(0) + \int_0^{L^a} \varphi^a dx = 0, & g_{4M+4} &= w^b\left(L^b\right) - w^b(0) + \int_0^{L^b} \varphi^b dx = 0, \\
g_{4M+5} &= \varphi^a\left(L^a\right) - \varphi^a(0) - \int_0^{L^a} \kappa^a dx = 0, & g_{4M+6} &= \varphi^b\left(L^b\right) - \varphi^b(0) - \int_0^{L^b} \kappa^b dx = 0, \\
g_{4M+7} &= -S_1^a - N^a(0) = 0, & g_{4M+8} &= -S_1^b - N^b(0) = 0, \\
g_{4M+9} &= -S_2^a - Q^a(0) = 0, & g_{4M+10} &= -S_2^b - Q^b(0) = 0, \\
g_{4M+11} &= -S_3^a - M^a(0) = 0, & g_{4M+12} &= -S_3^b - M^b(0) = 0, \\
g_{4M+13} &= S_4^a - N^a\left(L^a\right) = 0, & g_{4M+14} &= S_4^b - N^b\left(L^b\right) = 0, \\
g_{4M+15} &= S_5^a - Q^a\left(L^a\right) = 0, & g_{4M+16} &= S_5^b - Q^b\left(L^b\right) = 0, \\
g_{4M+17} &= S_6^a - M^a\left(L^a\right) = 0, & g_{4M+18} &= S_6^b - M^b\left(L^b\right) = 0.
\end{aligned} \tag{13}$$

The above system of non-linear algebraic equations of the side-plated beam comprises $4M+18$ equations for $4M+18$ primary unknowns ε_m^i, κ_m^i, $u^i(0)$, $w^i(0)$, $\varphi^i(0)$, $u^i(L)$, $w^i(L)$, $\varphi^i(L)$, $N^i(0)$, $Q^i(0)$, $M^i(0)$. Its solution is obtained by the Newton-Raphson method. Once the primary unknowns have been obtained, the secondary unknown functions, u^i, w^i, φ^i, N^i, Q^i, M^i, ΔU, ΔW, $P_{c,x}^i$, $P_{c,z}^i$, $M_{c,y}^i$ ($i = a, b$), are given at any particular value of x by the equations

$$
\begin{aligned}
u^i(x) &= u^i(0) + \int_0^x \varepsilon^i d\xi, \\
w^i(x) &= w^i(0) - \int_0^x \varphi^i d\xi, \\
\varphi^i(x) &= \varphi^i(0) + \int_0^x \kappa^i d\xi, \\
N^i(x) &= N^i(0) - \int_0^x \left(p_x^i + P_{c,x}^{\ i} \right) d\xi, \\
Q^i(x) &= Q^i(0) - \int_0^x \left(p_z^i + P_{c,z}^{\ i} \right) d\xi, \\
M^i(x) &= M^i(0) + \int_0^x \left(Q^i - m_y^i + M_{c,y}^{\ i} \right) d\xi, \\
\Delta U &= \left(u^b - u^a \right) + z\left(\varphi^b - \varphi^a \right), \\
\Delta W &= w^b - w^a, \\
P_{c,x}^{\ a} &= -P_{c,x}^{\ b} = F\ (\Delta U), \\
P_{c,z}^{\ a} &= -P_{c,z}^{\ b} = G\ (\Delta W), \\
M_{c,y}^{\ a} &= -M_{c,y}^{\ b} = H\ (\Delta U).
\end{aligned}
\tag{14}
$$

In the numerical formulation to be used in the analyses presented in the next section, the integrals in Eqs. (13) and (14) were evaluated numerically with the Gaussian numerical integration. The specific features of the present numerical formulation enables us to use any degree of the Lagrangian polynomials. The formulation also enables the point loading to be applied at the boundary nodes of each individual finite element.

4. Validation of the model and numerical examples

In the fourth section of the article, the present formulation is implemented in the mechanical analyses of two characteristic examples of externally plated beams. The objective of the first example (Section 4.1) is the validation of the model. The second numerical example (Section 4.2) carries out the comparisons between the two different arrangements of strengthening of the beam, i.e. the side-plated and the tension-face plated beams.

The finite elements employed in analyses of this section are denoted by E_{j-k}, where j indicates the number of the interpolation points and k the number of the Gaussian integration nodes along the element length.

Various material constitutive laws have been employed in the analyses. The bi-linear stress-strain relationship is used for the reinforcing steel bars and the steel side plates and material parameters given in the European building code EC2 (Eurocode 2 2005) are applied in all examples. Eurocode 2 (2005) is also used as a reference for the non-linear constitutive law of concrete in the second example (Section 4.2). In order to come as close as possible to the

experimental results, however, a somewhat different non-linear stress-strain relationship proposed by Desayi and Krishnan (1964) is implemented in the first example analysis (Section 4.1). When compared to the model provided by EC2, the model of Desayi and Krishnan suggests a slightly different definition of the constitutive law of the material and recommends a higher value of the ultimate concrete strain D_{cu}. This allows for taking into account the advantageous impact of the transverse reinforcement in formation of a beneficial spatial stress state, so that a more ductile behaviour of concrete is assured. In addition, the beneficial effect of the tensile strength of the concrete in accordance with Bergan and Holand (1979) is also incorporated in the analysis of the first example (Section 4.1). The above mentioned constitutive laws of steel and concrete are displayed in Fig. 2 and presented below by Eqs. (15)-(17).

- The stress-strain relation of concrete for structural analysis proposed by EC2 (2005)

$$\sigma_c(D_c)=\begin{cases}0 & \dots D_c < D_{cu}\\ -f_{cm}\dfrac{k\eta-\eta^2}{1+k\eta-2\eta} & \dots D_{cu}\le D_c\le 0,\\ 0 & \dots D_c>0\end{cases} \tag{15}$$

with $k=-1.05E_{cm}\dfrac{D_{c1}}{f_{cm}}$ and $\eta=\dfrac{D_c}{D_{c1}}$.

- The stress-strain relation of concrete of Desayi and Krishnan (1964) and Bergan and Holand (1979)

$$\sigma_c(D_c)=\begin{cases}0 & \dots D_c < D^*_{cu}\\ \dfrac{E_{c0}D_c}{1+\left(\dfrac{D_c}{D_{c1}}\right)^2} & \dots D^*_{cu}\le D_c\le D'_{cr}\\ \dfrac{D_{max}-D_c}{D_{max}-D'_{cr}}f'_{ct} & \dots D_{cr}<D_c\le D_{max}\\ 0 & \dots D_c>D_{max}\end{cases}, \tag{16}$$

with $E_{c0}=\dfrac{2f_{cm}}{D_{c1}}$, $D'_{cr}=0.55D_{cr}$, $D'_{cr}=0.1‰$, $D_{\max}=0.7‰$ and $D^*_{cu}=4.1‰$.

In Eqs. (15) and (16), D_c stands for the longitudinal strain of concrete, and D_{c1}, D_{cu}, E_{cm}, f_{cm}, and f_{ct} are, respectively, the concrete strain at peak stress, the concrete ultimate strain, the secant modulus of elasticity of concrete, and the absolute mean values of cylinder compressive and tensile strength of concrete at age 28 days, all of these values taken as proposed by EC2. D^* is the ultimate compressive strain of concrete as proposed by Desayi and Krishnan (1964).

- The stress-strain relation of steel proposed by EC2 (Eurocode 2 2005)

$$\sigma_s(D_s)=\begin{cases}E_sD_s & \dots|D_s|<D_{y1}\\ \left(f_y+E_p\left(|D_s|-D_{y1}\right)\right)\operatorname{sign}(D_s) & \dots D_{y1}\le|D_s|\le D_{y2}\\ \left(f_y+E_p\left(D_{y2}-D_{y1}\right)\right)\left(1-\dfrac{|D_s|-D_{y2}}{D_{yu}-D_{y2}}\right)\operatorname{sign}(D_s) & \dots D_{y2}\le|D_s|\le Du\\ 0 & \dots|D_s|>D_{yu}\end{cases}, \tag{17}$$

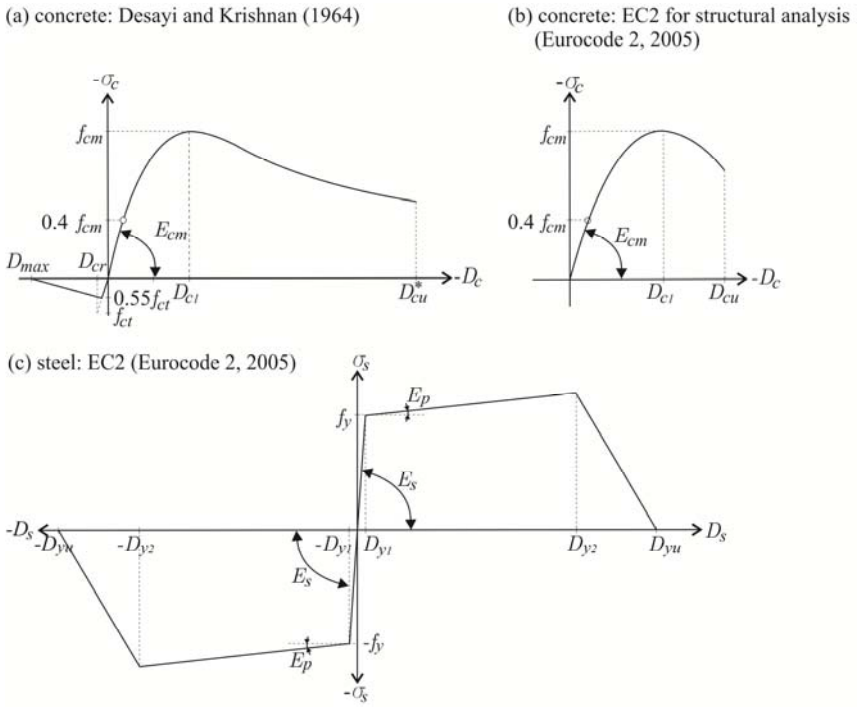

Fig. 2 Stress-strain relationships of: (a) concrete as proposed by Desayi and Krishnan (1964) and complemented by the strength contributions of concrete in tension in accordance with Bergan and Holand (1979) (implemented in the numerical example presented in Section 4.1); (b) concrete as proposed by Eurocode 2 (2005) appropriate for cases of structural analyses (implemented in the numerical example presented in Section 4.2); (c) steel as proposed by Eurocode 2 (2005) (implemented in the numerical examples presented in Sections 4.1 and 4.2)

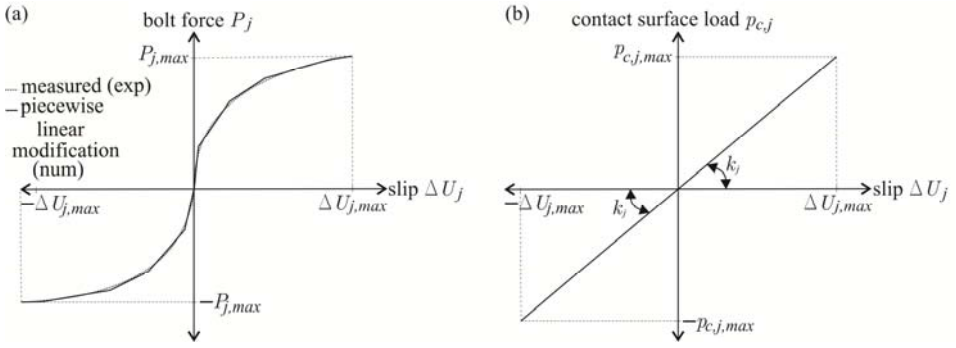

Fig. 3 Contact constitutive laws implemented in the mechanical analyses of beams presented in: (a) Section 4.1: Non-linear bolt force/deformation response of one bolt measured in a standard bolt shear test and its piecewise linear modification used in numerical simulations; (b) Section 4.2: Linear contact traction load/deformation response of the contact connection between the layers of the plated beam. The same contact relationship is assumed for both the longitudinal and the transversal directions ($j = x, z$)

where E_s stands for the modulus of elasticity of steel, E_p for the tangent modulus of steel hardening, f_y and D_{y1}, respectively, for the yield stress and the yield strain of steel, D_{y2} for the steel strain at the peak stress, and D_{yu} for the ultimate steel strain.

In concluding the preliminary part of this section, we present the contact constitutive laws to be used in the numerical analyses. In the numerical calculations of Section 4.1, a somewhat simplified piecewise linear modification (Fig. 3(a)) of the load/deformation response of the bolt as measured in a standard bolt shear test is employed as a simulation of the mechanical response of each individual bolt connecting the layers of the side-plated beam. In the numerical case of Section 4.2, the contact law of the interlayer connection is taken simply as linear (Fig. 3(b)). The same contact relationship is assumed for both the longitudinal and the transversal directions.

4.1 Simply supported RC beam with steel side plates

Our first numerical example is a simply supported reinforced concrete (RC) beam with a clear span of L = 360 cm and externally strengthened with two symmetrically bolted side plates. The beam is under a two-point bending with point loads 60 cm away from the midspan. This beam was tested experimentally by Su *et al*. (2010) and later on also computationally by Siu and Su (2011). Their results are used to verify the present numerical model extensively. The objective of the full-scale laboratory tests of Su *et al*. (2010) was to assess the influence of different side plates and different contact connections on the mechanical behavior of the tested flexural beam, therefore, different beam side plating variants were tried out. Here three of them marked as SBWP ('strong bolts-weak plate'), WBSP ('weak bolts-strong plate') and WBWP ('weak bolts-weak plate') will be

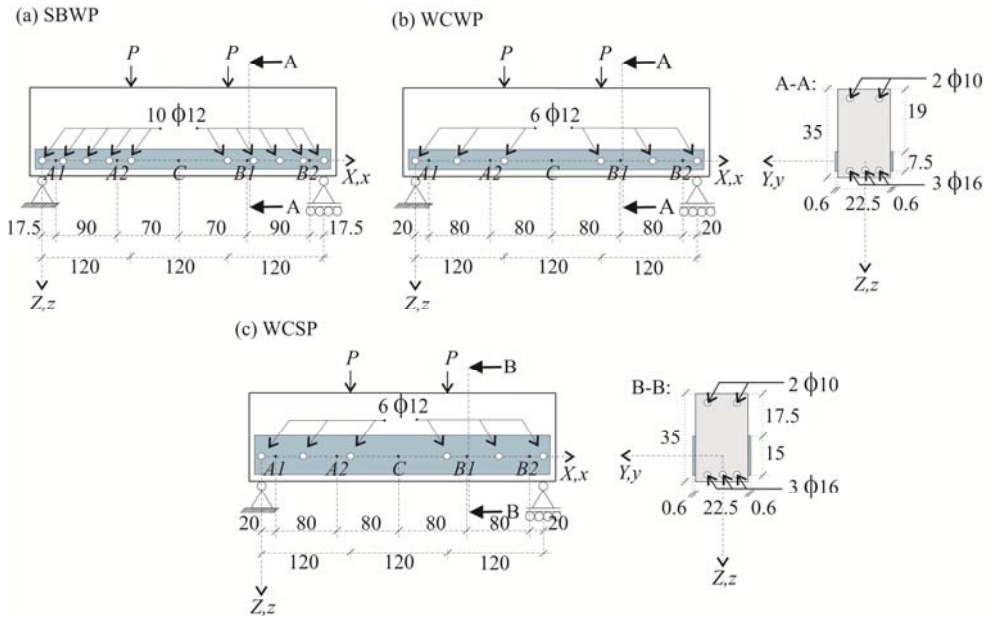

Fig. 4 Simply supported side-plated RC beam. The geometric properties (the side views and the typical cross- sections) and loading attributes (units of the diameters of the bars and the bolts are millimetres, units of the other length quantities are centimetres)

Table 1 Material properties of concrete

Concrete cube strength f_C [MPa]	Young's modulus E_C [GPa]	Cube strength strain D_{c1} [‰]	Ultimate strain D_{cu} [‰]
34.30	32.30	2.00	3.50

Table 2 Material properties of the steel strengthening plates and the reinforcing steel bars

	Yield strength f_y [MPa]	Young's modulus E_S [GPa]	Yield strain D_y [‰]	Ultimate strain D_t [‰]
plates	355.00	212.00	1.58	20.00
bars	537.00	187.00	1.58	20.00

presented. The geometric (the side-views and the cross-sections) as well as the loading data of the three beams are given in Fig. 4. The material properties data (Su *et al*. 2010, Siu and Su 2010) used in the calculations are presented in Tables 1 and 2.

A comparisons between the experimental (Su *et al*. 2010, Siu and Su 2010) and the computational results (Siu and Su 2011) and the present results are shown in Figs. 5 and 6. First, load-deflection responses are depicted in Fig. 5. It is clear that the agreement between the experimental ('–') and the present numerical data ('o') is good. The present numerical formulation predicted the failure of the WBSP and WBWP triggered by the fracture of the two bolts closest to the support, whereas the SBWP beam (with a weaker plate but also a stronger contact connection) would fail in concrete crushing. The collapse simulations agree with the experimentally observed results (Su *et al*. 2010). In addition, the bearing capacities observed by the experiments and those predicted by the present numerical formulation seem to agree well with the errors ranging only roughly from 0.7% to 1%. Well simulated seem to be also the stiffness and the ductility of the beams and also the turning points in the ascending parts of the curves corresponding to the instants, when yielding of the bottom reinforcement takes place (the detected errors range from roughly −1.5% to 3.2%). Some further details regarding the differences between the present and the experimental results are given in Table 4.

The differences between the present numerical results ('o') and the numerical simulations of Siu and Su ('...') are also only minor. They probably come from the different stress-strain laws of concrete used in the two models. While Siu and Su assumed the concrete constitutive law having a constant stress in the post-peak region ($\sigma_c = f_{cm}$ for $D_c > D_{c1}$), the present numerical model adopted a law with a descending post-peak region and considered the advantageous effect of the transversal reinforcement on the ductility of the beam. The consequences of such choices are especially noticeable in the improved ductility of the structural response predicted by the present numerical model in the case of the beam SBWP (Fig. 5(a)). Furthermore, the bearing capacity of concrete in tension was ignored in the numerical simulation of Siu and Su (2011). These differences result in deviations in both the initial stiffness of the load-deflection curves and the ultimate bearing capacity of the beam. For a detailed presentation of the effect of the tensile strength of concrete observe Table 3. The table shows the present numerical results for: (i) when tensile strength of concrete is accounted for in the analysis; and (ii) when it is neglected. Initially (see midspan deflection at the load level MC = 48 kNm), a somewhat higher stiffness of the structural response

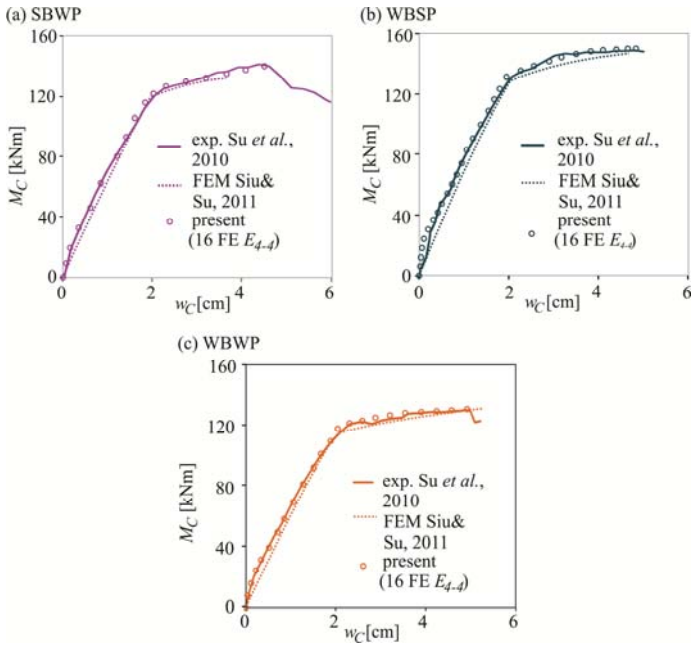

Fig. 5 Simply supported side-plated RC beam. A comparison of moment-deflection responses between the experimental results of Su *et al*. (2010) ('–'), the numerical results of Siu and Su (2011) ('...') and the present numerical results ('o') for three plating arrangements: (a) SBWP; (b) WBSP; and (c) WBWP

Table 3 A comparison between the present numerical results for the initial stiffness (which is demonstrated by the midspan deflection at the load level M_C = 48 kNm), ultimate bearing capacity M_C^u, and the ultimate midspan deflection w_C^u of the beams WBSP, SBWP, and WBWP for: (i) when the tensile strength of concrete is accounted for in the analysis; and (ii) when it is neglected

	w_C (M_C = 48kNm) [cm]		M_C^u [kNm]		w_C^u [cm]	
	(i)	(ii)	(i)	(ii)	(i)	(ii)
WBSP	0.5628	0.6169	154.01	153.80	5.3301	5.2371
SBWP	0.6680	0.7119	139.58	139.37	4.6711	4.6194
WBWP	0.6679	0.7117	135.38	134.58	4.6710	4.3969

is observed for the case (i). In addition, a somewhat higher ultimate bearing capacity of the beam is obtained for this case. From the point of view of engineering purposes, both of the two differences are, however, rather insignificant.

The longitudinal slip responses of the observed beams are depicted in Fig. 6 ('–' and '-.-' – experimental results, '...' - numerical results of Siu and Su, 'o' – the present numerical results). Only small differences between the two numerical results can be detected. These differences correctly reflect the distinctions between the bolt force/slip responses implemented in the models.

Recall that Siu and Su assumed a simplified bi-linear relationship with a somewhat stiffer initial part and a more flexible final part of the curve, in contrast to the more precise bolt model as implemented in the present analysis (see Fig. 4). Nonetheless, these deviations are insignificant throughout the response of the beam, and idicates that Siu and Su's assumption of bi-linearity of the bolt force-slip response is reasonable and accurate enough for engineering purposes.

The comparison of slips obtained in the numerical and the experimental results indicates lower experimentally measured slips as a rule. As already discussed by Siu and Su (2011), the difference may be due to the fact that the frictional resistance between the surfaces of the beam and the side plates is ignored in the analyses.

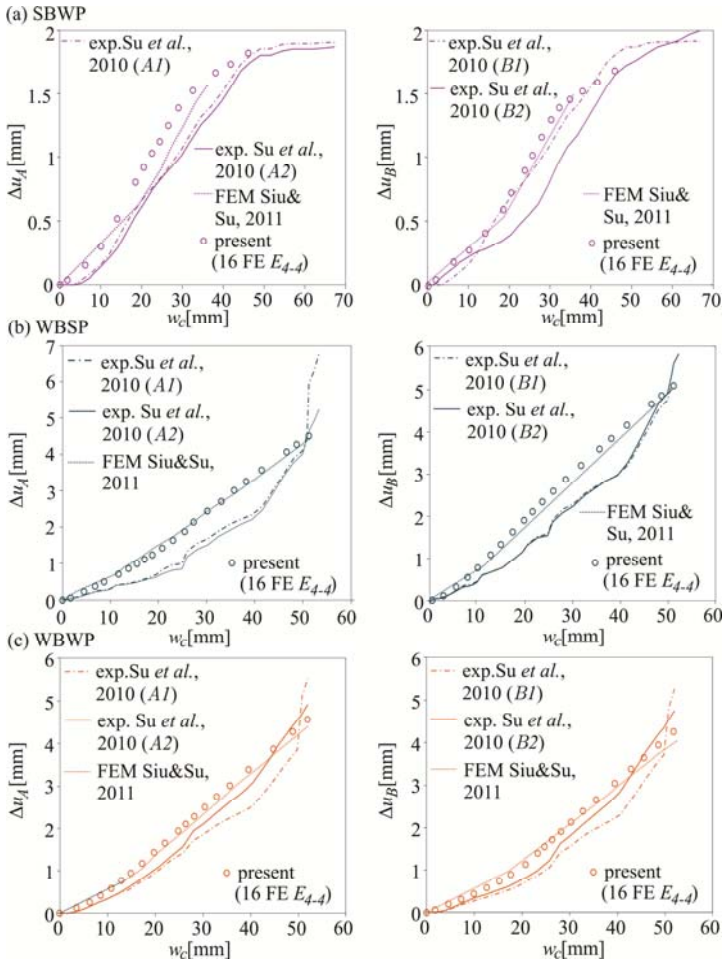

Fig. 6 Simply supported side-plated RC beam. A comparison of mid-span deflection/longitudinal slip (absolute values) in points *A*1, *A*2, *B*1 and *B*2 (for the positions of the points, see Fig. 4) between the experimental results of Su *et al*. (2010) ('–' - slips at positions '1' and '-.-' - slips at positions '2'), the numerical results of Siu and Su (2011) ('...') and the numerical results of the present formulation ('o') for three plating variants: (a) SBWP; (b) WBSP; and (c) WBWP. Due to the planar deformation assumed in the numerical analysis, the computed slips for both plates are the same

Table 4 Errors of the present numerical calculations in the predicted bending moment, $M^{y}_{C,p}$, at the first yielding of the bottom reinforcement, and of the predicted peak bending moment, $M^{u}_{C,p}$, with respect to the experimental results of Su *et al*. (2010). ($\Delta M^{y}_{C} = M^{y}_{C,\exp} - M^{y}_{C,p}$, $\Delta M^{u}_{C} = M^{u}_{C,\exp} - M^{u}_{C,p}$; '*p*' stands for '*present*' and '*exp*' for '*experiment*')

	$\frac{\Delta M^{y}_{C}}{M^{y}_{C,\exp}} * 100\%$	$\frac{\Delta M^{u}_{C}}{M^{u}_{C,\exp}} * 100\%$
SBWP	3.23	0.69
WBSP	-1.50	1.21
WBWP	-1.04	1.04

Table 5 Material properties of concrete

Concrete cube strength f_C [MPa]	Young's modulus E_C [GPa]	Cube strength strain D_{c1} [‰]	Ultimate strain D_{cu} [‰]
38.30	33.60	2.00	3.50

Table 6 Material properties of the steel strengthening plates and the reinforcing steel bars

Yield strength f_Y [MPa]	Young's modulus E_S [GPa]	Yield strain D_y [‰]	Ultimate strain D_t [‰]
465.00	200.00	2.30	20.00

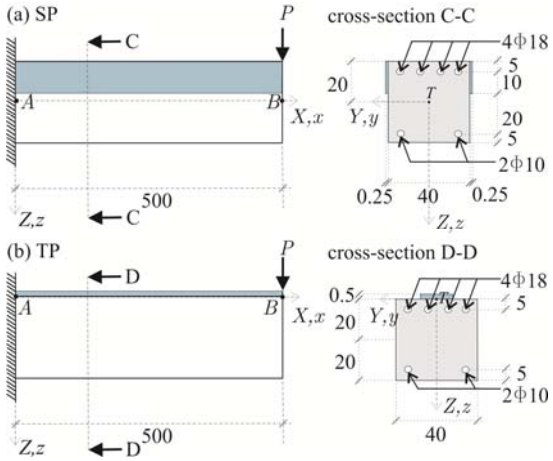

Fig. 7 RC cantilever beam: geometric properties, typical cross-sections and loading data for two different examples of external strengthening of the beam: (a) side strengthening; and (b) tensile-face strengthening. The diameters of the bars are given in millimetres, units of the remaining length quantities are centimetres

4.2 RC cantilever beam with side and tension-face plates

The aim of this section is to compare the side plating strengthening method with the alternative tension-face plating method. We explore the ductility, bearing capacity and the stiffness of the

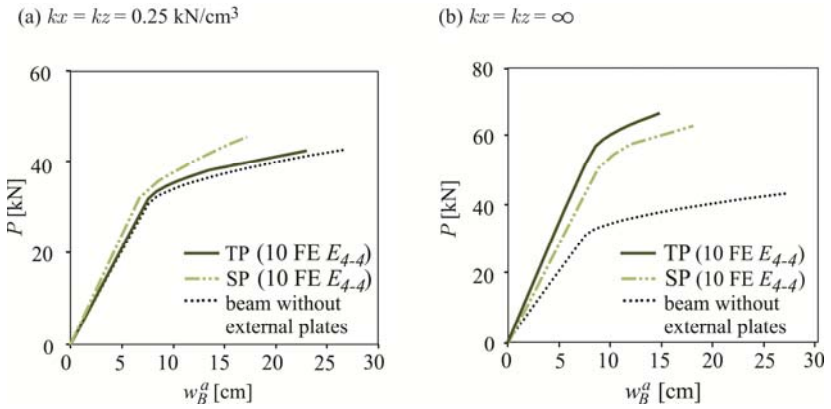

Fig. 8 Force-deflection responses of two externally strengthened RC cantilever beams for two different connection stiffnesses: (a) flexible contact connection ($k_x = k_z = 0.25$ kN/cm^3) and (b) stiff contact connection $k_x = k_z = \infty$ kN/cm^3). Full lines ('–') represent the numerical results of tension-face plated beams. Dash-dotted lines ('-..-') signify numerical results of the alternative side-plated beams. Dotted lines ('...') mark the results for a beam with no external strengthening

side-plated (SP) and the tension-face plated (TP) RC cantilever beam of length 500 cm (Fig. 7). The response of the tensile-face plated beam was obtained by the numerical model of Kroflič *et al*. (2010b). The contact law was taken to be linear, yet two differently stiff interlayer connections were applied: $k_x = k_z = 0.25$ kN/cm^3 (modelling a flexible contact) and $k_x = k_z = \infty$ kN/cm^3 (modelling a stiff contact). The material properties of concrete and steel reinforcement (the steel strengthening plates and the steel reinforcement bars) are presented in Tables 5 and 6. The remaining data are shown in Fig. 7.

Fig. 8 depicts the load-deflection responses of the side-plated ('-..-') and the tension-face plated ('–') beams. Which type of plating is more effective depends on the stiffness of the connection. In fact, in the case of the stiff connection (see the results in Fig. 8(b)), the tension face strengthening enhances strength more than the side-plate one, yet the ductility becomes smaller. Just the opposite holds true, if the connection is sufficiently flexible (see the results in Fig. 8(a)). Note a substantial increase in the bearing capacity for the stiff connection for both types of strengthening.

5. Conclusions

We have presented a new mathematical model and its finite element numerical solution of the geometrically linear side-plated planar beam with a fully non-linear material beam/side plate contact connection flexible in both the longitudinal and the transversal direction. The material properties are assumed to be non-linear and can include combinations like FRP–concrete and steel–concrete often met in structural engineering. The governing equations of the model have been discretized by the strain-based finite element method where only the extensional strain and the curvature are interpolated. The verification of the model has been performed by the comparison of the present solution with other numerical as well as experimental results from literature. Our results indicate that the presented numerical formulation is very accurate and the

outcomes reliable, which proves that the present method is a suitable tool for the mechanical analysis of side-plated members. The present solution has been employed in exploring the effects of different strengthening on the bearing capacity and ductility of a cantilever beam. The comparisons have been made between the tension-face plating and the side plating arrangements. The analysis revealed that the side plates can indeed efficiently enhance the bearing capacity of the unstrengthened beam, which can, under some conditions, exhibit a lower loss of ductility. If the connection is sufficiently flexible, the side-plated strengthening may well outperform in strength the tension-face strengthening.

Acknowledgments

The work of J. Kolšek was partly financially supported by the European Union, European Social Fund. The support is gratefully acknowledged.

References

Ahmed, M. (1996), "Strengthening of reinforced concrete beams by bolting steel plates to their sides", Master of Engineering Science Thesis, The University of Adelaide, Australia.

Alfano, G. and Crisfield, M.A. (2001), "Finite element interface models for the delamination analysis of laminated composites: mechanical and computational issues", *Int. J. Numer. Method. Eng.*, **50**(7), 1701-1736.

Bergan, P.G. and Holand, I. (1979), "Nonlinear finite element analysis of concrete structures", *Comput. Methods Appl. Mech. Eng.,* **17-18**(2), 443-467.

Čas, B., Saje, M. and Planinc, I. (2004a), "Non-linear finite element analysis of composite planar frames with an interlayer slip", *Comput. Struct.*, **82**(23-26), 1901-1912.

Čas, B., Saje, M. and Planinc, I. (2004b), "Non-linear analysis of composite steel-concrete beams with incomplete interaction", *Steel Compos. Struct.*, *Int. J.*, **4**(6), 489-507.

Eurocode 2 (2005), ENV 1992-1-1, Eurocode 2: Design of concrete structures - Part 1-1: General rules and rules for buildings, Brussels, Belgium.

Desayi, P. and Krishnan, S. (1964), "Equation for the stress–strain curve of concrete", *J. Am. Concr. Inst.* **61**(3), 345-350.

Gara, F., Ranzi, G. and Leoni, G. (2006), "Displacement based formulations for composite beams with longitudinal slip and vertical uplift", *Int. J. Numer. Method. Eng.*, **68**(8), 1197-1220.

Hjelmstad, K.D. (2005), *Fundamentals of Structural Mechanics*, (2nd Edition), Springer (India) Pvt. Ltd., New Delhi, India.

Kolšek, J., Hozjan, T., Saje, M. and Planinc, I. (2013), "Analytical solution of linear elastic beams cracked in flexure and strengthened with side plates", *J. Compos. Mater.*, **47**(22), 2847-2864.

Kroflič, A., Planinc, I., Saje, M. and Čas, B. (2010a), "Analytical solution of two-layer beam including interlayer slip and uplift", *Struct. Eng. Mech.*, *Int. J.*, **34**(6), 667-683.

Kroflič, A., Planinc, I., Saje, M., Turk, G. and Čas, B. (2010b), "Non-linear analysis of two-layer timber beams considering interlayer slip and uplift", *Eng. Struct.*, **32**(6), 1617-1630.

Liu, I.S.T., Oehlers, D.J. and Seracino, R. (2006), "Tests on the ductility of reinforced concrete beams retrofitted with FRP and steel near surface mounted plates", *J. Compos. Construct.*, **10**(2), 106-114.

Milner, H.R. and Tan, H.H. (2001), "Modelling deformation in nailed, thin-webbed timber box beams", *Comput. Struct.*, **79**(29-30), 2541-2546.

Nguyen, N.T., Oehlers, D.J. and Bradford, M.A. (2001), "An analytical model for reinforced concrete beams with bolted side plates accounting for longitudinal and transverse partial interaction", *Int. J. Solid. Struct.*, **38**(38-39), 6985-6996.

Oehlers, D.J., Ahmed, M., Nguyen, N.T. and Bradford, M.A. (2000), "Retrofitting reinforced concrete beams by bolting steel plates to their sides. Part 2. Transverse interaction and rigid plastic design", *Struct. Eng. Mech., Int. J.*, **10**(3), 227-243.

Oehlers, D.J., Nguyen, N.T., Ahmed, M. and Bradford, M.A. (1997), "Transverse and longitudinal partial interaction in composite bolted side-plated reinforced-concrete beams", *Struct. Eng. Mech., Int. J.*, **5**(5), 553-564.

Oehlers, D.J. and Seracino, R. (2004), *Design of FRP and Steel Plated RC Structures*, Elsevier, Oxford, UK.

Planinc, I., Saje, M. and Čas, B. (2001), "On the local stability condition in the planar beam finite element", *Struct. Eng. Mech., Int. J.*, **12**(5), 507-526.

Pan, J.L. and Leung, C.K.Y. (2008), "Effect of end tapering on crack-induced FRP debonding from the concrete substrate", *J. Compos. Construct.*, **12**(1), 15-24.

Ranzi, G., Gara, F. and Ansourian, P. (2006), "General method of analysis for composite beams with longitudinal and transverse partial interaction", *Comput. Struct.*, **84**(31-32), 2373-2384.

Reissner, E. (1972), "On one-dimensional finite-strain beam theory: The plane problem", *J. Appl. Math. Phys.*, **23**(5), 795-804.

Schnabl, S., Planinc, I., Saje, M., Čas, B. and Turk, G. (2006), "An analytical model of layered continuous beams with partial interaction", *Struct. Eng. Mech., Int. J.*, **22**(3), 263-278.

Schnabl, S., Saje, M., Turk, G. and Planinc, I. (2007), "Analytical solution of two-layer beam taking into account interlayer slip and shear deformation", *J. Struct. Eng.*, **133**(6), 886-894.

Siu, W.H. and Su, R.K.L. (2010), "Effects of plastic hinges on partial interaction behaviour of bolted side-plated beams", *J. Construct. Steel Res.*, **66**(5), 622-633.

Siu, W.H. and Su, R.K.L. (2011), "Analysis of side-plated reinforced concrete beams with partial interaction", *J. Construct. Steel Res.*, **66**(5), 622-633.

Smith, S.T., Bradford, M.A. and Oehlers, D.J. (1999a), "Local buckling of side-plated reinforced-concrete beams. I: Theoretical study", *Comput. Concrete*, **8**(1), 71-96.

Smith, S.T., Bradford, M.A. and Oehlers, D.J. (1999b), "Local buckling of side-plated reinforced-concrete beams. II: Experimental study", *J. Struct. Eng.*, **125**(6), 635-643.

Su, R.K.L., Siu, W.H. and Smith, S.T. (2010), "Effects of bolt-plate arrangements on steel plate strengthened reinforced concrete beams", *Eng. Struct.*, **32**(6), 1769-1778.

Thomsen, H., Spacone, E., Limkatanyu, S. and Camata, G. (2004), "Failure mode analyses of reinforced concrete beams strengthened in flexure with externally bonded fiber-reinforced polymers", *J. Compos. Construct.*, **8**(2), 123-131.

CC